

# Large Magnetic Anisotropy of a Single Atomic Spin Embedded in a Surface Molecular Network

Cyrus F. Hirjibehedin,<sup>1</sup> Chiung-Yuan Lin,<sup>1,2</sup> Alexander F. Otte,<sup>1,3</sup> Markus Ternes,<sup>1,4</sup> Christopher P. Lutz,<sup>1</sup> Barbara A. Jones,<sup>1</sup> Andreas J. Heinrich<sup>1</sup>

Magnetic anisotropy allows magnets to maintain their direction of magnetization over time. Using a scanning tunneling microscope to observe spin excitations, we determined the orientation and strength of the anisotropies of individual iron and manganese atoms on a thin layer of copper nitride. The relative intensities of the inelastic tunneling processes are consistent with dipolar interactions, as seen for inelastic neutron scattering. First-principles calculations indicate that the magnetic atoms become incorporated into a polar covalent surface molecular network in the copper nitride. These structures, which provide atom-by-atom accessibility via local probes, have the potential for engineering anisotropies large enough to produce stable magnetization at low temperatures for a single atomic spin.

<sup>1</sup> IBM Research Division, Almaden Research Center, San Jose, CA 95120, USA.

<sup>2</sup> Center for Probing the Nanoscale, Stanford University, Stanford, CA 94309, USA.

<sup>3</sup> Kamerlingh Onnes Laboratorium, Universiteit Leiden, 2300 RA Leiden, Netherlands.

<sup>4</sup> Institut de Physique des Nanostructures, École Polytechnique Fédérale de Lausanne, 1015 Lausanne, Switzerland.

To whom correspondence should be addressed. E-mail: [heinrich@almaden.ibm.com](mailto:heinrich@almaden.ibm.com)

Magnetic structures with only a few atomic spins, such as single atoms and clusters on metal surfaces ([1](#), [2](#)) and molecular magnets ([3–5](#)), can exhibit anisotropies that are large enough to maintain a stable spin orientation at low temperatures. The large anisotropies per each atom in these small clusters are of interest as a possible way to shrink magnetic bits below the size at which domains in current thin-film magnetic materials become unstable at room temperature. The impending approach of this superparamagnetic limit ([6](#)) threatens to halt the decades-long trend toward ever higher storage densities in magnetic memory. Besides this technological relevance, atomic-scale magnetic structures are also of great scientific interest because they exhibit intriguing quantum effects ([7–9](#)) and have the potential to be harnessed for quantum computing ([10](#), [11](#)). Access to individual magnetic nanostructures by electronic transport measurements is possible with the use of electromigration junctions ([12](#), [13](#)) and local probes ([2](#), [14–18](#)). Whereas nanoscale junction devices may be more readily adapted to practical applications, studies using local probes provide an understanding of the nanomagnet's local environment, the crucial determinant of atomic-scale anisotropy.

Here we describe magnetic nanostructures with large magnetic anisotropy that can be individually constructed, studied, and manipulated with atomic-scale precision. Individual Fe or Mn atoms were placed at the desired locations on a CuN surface by manipulation with a scanning tunneling microscope (STM) tip. Our calculations indicate that the Fe and Mn atoms are embedded into a molecular network of polar covalently bonded Cu and

N atoms within the CuN surface. Incorporation into the surface results in substantial charge transfer and distribution of spin polarization away from the magnetic atom and into the molecular network. We found that inelastic excitations of the atomic spin ([14](#), [15](#)) are very prominent in the electron tunneling from an STM tip through the individual magnetic nanostructures. Changes in the spin-excitation energies as a magnetic field was applied along three orthogonal axes directly yielded both the strength and orientation of axial and transverse magnetic anisotropy for a single magnetic atom. The relative intensities of these inelastic excitations are well-described by a spin-transition matrix element that is analogous to that found in inelastic neutron scattering. These nanomagnetic systems combine large magnetic anisotropies with the flexibility that comes from being accessible on a surface by a local probe ([2](#), [14–18](#)) and the potential for control of the magnetic properties previously available only in molecular magnets. This has great promise because, in the absence of transverse anisotropy, the single Fe atom on CuN would have an energy-reversal barrier similar in magnitude to that observed for atomic spins in the most anisotropic configurations in molecular magnets ([4](#)) and on metal surfaces ([1](#)).

Experiments were conducted with an ultra high-vacuum low-temperature STM with a base temperature of 0.5 K. We measured the differential conductance  $dI/dV$  using lock-in detection of the tunnel current  $I$  by adding a 20- to 50- $\mu\text{V}_{\text{rms}}$  modulation at  $\sim 800$  Hz to the sample bias voltage  $V$  [we used the root mean square (rms) amplitude for the modulation voltage]. The STM head was mounted in the cold bore of a split-coil magnet with magnetic fields  $B$  up to 7 T. The orientation of the magnet could be changed so that the magnetic field was applied either perpendicular to or in the plane of the crystal surface ([19](#)).

We used a single atomic layer of CuN ([20](#)) to decouple the spin of the magnetic atoms from the conduction electrons in the underlying Cu(100) surface ([15](#)). A small island of CuN with an adsorbed Fe atom is shown in [Fig. 1A](#). As seen in the cross section, the Fe atom has a large apparent height of 2.6 Å, which indicates that electronic tunneling through the atom is almost three orders of magnitude greater than it is through the bare CuN. The spatial resolution of the STM images, particularly the observation of single rows of missing N atoms such as those shown in [Fig. 1A](#), allowed us to overlay the lattice structure and determine the binding site of the atom and its local environment: In [Fig. 1A](#), the Fe is on top of a Cu atom with two N atoms as its horizontal nearest neighbors ([21](#)).

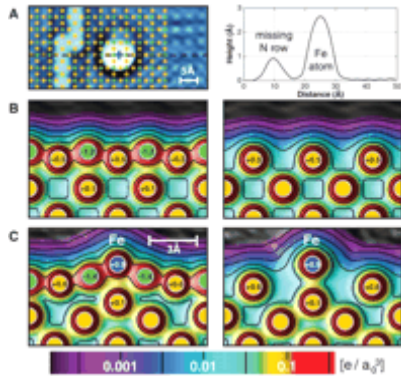


**Fig. 1.** Fe atoms on CuN. (A) (Left) Processed (37) constant-current topograph (10 mV, 0.5 nA) of two adjacent CuN islands with a single adsorbed Fe atom. The topograph is negative-curvature (high-pass) filtered to enhance contrast, with lattice positions of Cu (yellow dots) and N (green dots) atoms overlaid. The light vertical features on the left side of the image are formed by the absence of single rows of N atoms from the CuN surface. The topographic peak of the Fe atom (blue cross) shows its binding site: on top of a Cu site with two N atoms as horizontal neighbors. (Right) Cross section of the unfiltered topograph along the dashed line indicated in the left panel. (B) The charge density for a CuN surface on Cu(100) calculated with the DFT methods described in the text along the N (left) and hollow (right) directions. The scale for the magnitude of the charge density is shown at the bottom in units of  $e/a_0^3$ . Solid yellow and green circles with gray edges label the centers of the Cu and N atoms, respectively. The numbers inside the circles indicate the net charge on selected atoms in units of  $e$  (25). (C) Same as (B) with an Fe atom (blue) adsorbed on the CuN on top of a surface Cu site. [\[View Larger Version of this Image \(96K GIF file\)\]](#)

To understand the structure formed by magnetic atoms on the CuN surface, we calculated the electronic structure using the all-electron full-potential linearized augmented plane wave method of density functional theory (DFT) (22) with the exchange-correlation potential in the generalized gradient approximation (GGA) (23). Figure 1B shows cross sections of the calculated charge density for a single layer of CuN on Cu(100) (24) along two orthogonal directions in-plane: (i) the direction defined by the axis along two nearest-neighbor N atoms (which we refer to below as the N direction) and (ii) the direction along the axis defined by two nearest-neighbor hollow sites (the hollow direction). As seen in the cross sections, the N atoms are slightly above the plane of the surface Cu atoms. In addition, there is a net transfer of charge from the Cu atoms to the N atoms (25). A comparison of the charge densities along the two orientations shows that the CuN has formed a network of polar covalent bonds along the N rows that is distinct from the underlying bulk Cu.

Placing an Fe or Mn atom on top of a Cu atom in the CuN surface causes a substantial rearrangement of the atomic structure. As seen in Fig. 1C for Fe, the Cu atom directly below the magnetic atom has moved toward the bulk and is no longer part of the polar covalent CuN network. The magnetic atom transfers charge to the CuN surface and

creates bonds with its neighboring N atoms; the magnetic atom is thus incorporated into the extended molecular network on the surface. In spite of these extensive structural changes, we can reversibly attach and remove both Fe and Mn atoms from the CuN surface with the STM tip using a previously described technique (15).

The conductance spectra obtained over two different Fe atoms on different CuN islands at various in-plane magnetic fields are shown in Fig. 2, A and B. At  $B = 0$ , three clear steps are seen centered at  $|V_0| \cong 0.2, 3.8,$  and  $5.7$  mV (26). In the framework of inelastic electron tunneling spectroscopy (IETS) (27), these steps in conductance are interpreted as the opening of an inelastic tunneling channel associated with the creation of an excitation at energy  $eV_0$ , where  $e$  is the magnitude of the electron charge and  $V_0$  is the center of the step. Changes in energy and intensity of these excitations as a function of  $B$  allow us to assign them to spin excitations (14, 15). For a single orientation of  $B$ , the atoms were placed at different Cu sites on the surface so that the field was oriented along two different spatial directions: the N direction (for the atom in Fig. 2A) and the hollow direction (Fig. 2B). The existence of zero-field excitations indicates that the different spin orientations (quantum number  $m$ ) are nondegenerate even in the absence of a magnetic field, suggesting the presence of strong magnetic anisotropy in the system even for a single atomic spin on the CuN surface. Surprisingly large magnetic anisotropies have also been observed for isolated metal atoms on bare metal surfaces (1).

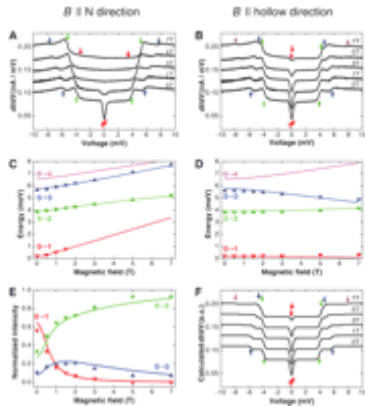


**Fig. 2.** Conductance spectra of Fe atoms on CuN. (A) Spectra taken with the STM tip positioned above an Fe atom at  $T = 0.5$  K and  $B = 0$  to 7 T oriented in the N direction. The spectra were acquired at a nominal junction impedance of 10 megohm (10 mV, 1 nA) and were not sensitive to junction impedance. Successive spectra are vertically offset by 0.023 nA/mV for clarity. Red, green, and blue upward arrows indicate the positions of the first, second, and third excitations, respectively, at  $B = 0$  T as calculated by Eq. 1 with the fit parameters described in the text. Downward arrows show the same excitations at  $B = 7$  T with the magnetic field oriented along the  $z$  axis of Eq. 1. (B) Same as (A) with  $B$  oriented along the hollow direction for the spectra; this direction corresponds to the  $x$  axis of Eq. 1. Also included are magenta downward arrows indicating the calculated position of the fourth transition at  $B = 7$  T. (C) Energies for the first (red triangles), second (green circles), and third (blue triangles) steps observed in the spectra acquired with  $B$  along the N direction, including those shown in (A). Solid lines indicate excitation energies calculated by

Eq. 1 with the magnetic field oriented along the  $z$  axis. **(D)** Step energies for the spectra acquired with  $B$  along the hollow direction, which corresponds to the  $x$  axis of Eq. 1, including those shown in **(B)**. **(E)** Relative step heights for the first (red), second (green), and third (blue) excitations as a function of  $B$  along the N direction. The individual step heights are normalized by the sum of the three step heights at each value of  $B$ . The fourth excitation is not included because its intensities are negligible in this range of  $B$ . Solid lines denote normalized transition intensities calculated using Eq. 2 with the fit parameters discussed in the text. **(F)** Simulated spectra, as described in the text, with  $B$  along the hollow direction and an effective temperature of 0.8 K. Arrows are the same as in **(B)**. These spectra are scaled by an overall constant and offset to match those shown in **(B)**. a.u., arbitrary units. [\[View Larger Version of this Image \(39K GIF file\)\]](#)

In [Fig. 2, C and D](#), the evolution of the energies of the IETS steps seen in [Fig. 2, A and B](#), is shown. The changes in the excitation energies are markedly different when the magnetic field is applied in the two different directions: When  $B$  is along the N direction ([Fig. 2C](#)), all of the step energies increase with  $B$ , whereas the first and third steps decrease in energy when  $B$  is applied along the hollow direction ([Fig. 2D](#)). At a given in-plane magnetic field, it was possible to move an individual Fe atom back and forth between the two distinct binding sites (i.e., sites so that  $B$  was oriented along either the N or hollow direction) and observe that the excitation spectrum switched correspondingly. These differences can be unambiguously observed only because we can probe individual magnetic atoms in a well-characterized environment. A third distinct behavior is seen when the magnetic field is applied in the out-of-plane direction on a different Fe atom, as illustrated in [fig. S1 \(28\)](#); in this case, very little change of the step energies is observed. This strong dependence of the spin excitations on field direction is further evidence of strong magnetic anisotropy for the Fe spin.

To lowest order, spin excitations in an anisotropic environment can be described by the spin Hamiltonian [\(5\)](#)

$$\hat{H} = g\mu_B \vec{B} \cdot \hat{S} + DS_z^2 + E(S_x^2 - S_y^2) \quad (1)$$

Here the first term is the Zeeman splitting of the states in the presence of a magnetic field, where  $g$  is the  $g$ -factor,  $\mu_B$  is the Bohr magneton, and  $\hat{S} = (\hat{S}_x, \hat{S}_y, \hat{S}_z)$  is the spin operator.

The second and third terms are phenomenological representations of the axial and transverse magnetic anisotropies, characterized by strengths  $D$  and  $E$ , respectively. The axial term splits the degeneracy of the spin-states on the basis of the magnitude of the spin's  $z$  projection  $m$ , whereas the transverse term mixes states of different  $m$ . By convention, the axes are assigned in Eq. 1 to maximize  $|D|$  and have  $E > 0$ .

Diagonalization of Eq. 1 allows us to calculate the excitation spectrum for the spin system. Using the spin of a free Fe atom ( $S = 2$ ) (29), a best fit of all of the excitations shown in Fig. 2, C and D, and fig. S1B (28) yields  $g = 2.11 \pm 0.05$ ,  $D = -1.55 \pm 0.01$  meV, and  $E = 0.31 \pm 0.01$  meV; here the uncertainties are the standard errors produced by the best fit.  $D < 0$  favors high  $|m|$  states, which are desirable for achieving magnetic bistability with a long lifetime (4). However, the relatively large transverse  $E$  term mixes the different spins states, making these structures unsuitable for use as bistable spin systems. It may be possible to remove such mixing by engineering the local environment of the atomic spin, for example, by positioning the magnetic atom on a surface site with higher symmetry. Similar magnetic-anisotropy values, although usually with positive  $D$  (corresponding to planar or hard-axis anisotropy), have been observed in studies of crystals formed from molecular magnet structures with single Fe atoms (30).

Figure 2, C and D, and fig. S1B (28) show the agreement between the observed IETS step energies and the excitation energies calculated from Eq. 1 as a function of  $B$ . In these calculations, the direction of  $B$  along the N, hollow, and out-of-plane directions is associated with the  $z$ ,  $x$ , and  $y$  axes in Eq. 1, respectively. A fourth excitation at a higher energy is also predicted to occur. Although no indication of this excitation is observed for  $B$  along the N and out-of-plane directions, a weak conductance step at the predicted energies is observed at larger magnetic fields applied along the hollow direction, as seen in Fig. 2B. Unexpectedly, the primary anisotropy axis (corresponding to the  $z$  axis in Eq. 1) is not directed out-of-plane but rather along the inplane N direction (i.e., along the direction of the CuN molecular network). This result indicates the importance of the local molecular-bonding environment in determining the magnetocrystalline anisotropy.

To better understand the inelastic tunneling process that governs the spin excitations observed with IETS, we also analyzed the intensity of the transitions as a function of magnetic-field strength and orientation. In Fig. 2E, the relative intensities of the three strong IETS steps as a function of  $B$  along the N direction are shown. We found that the relative IETS step heights for transitions between an initial spin eigenstate  $\psi_i$  and a final spin eigenstate  $\psi_f$  are well-described by

$$I_{i \rightarrow f} = \left| \langle \Psi_f | \hat{S}_x | \Psi_i \rangle \right|^2 + \left| \langle \Psi_f | \hat{S}_y | \Psi_i \rangle \right|^2 + \quad (2)$$

$$\begin{aligned}
& \left| \langle \Psi_f | \hat{S}_z | \Psi_i \rangle \right|^2 \\
&= \frac{1}{2} \left[ \left| \langle \Psi_f | \hat{S}_+ | \Psi_i \rangle \right|^2 + \left| \langle \Psi_f | \hat{S}_- | \Psi_i \rangle \right|^2 + \right. \\
& \quad \left. 2 \left| \langle \Psi_f | \hat{S}_z | \Psi_i \rangle \right|^2 \right]
\end{aligned}$$

where  $\hat{S}_\pm = \hat{S}_x \pm i \hat{S}_y$  (here,  $i = \sqrt{-1}$ ) and  $\psi_i$  and  $\psi_f$  are obtained directly from the diagonalization of Eq. 1. As shown in [Table 1](#),  $\psi_0$  has most of its weight in the  $|m = +2\rangle$  and  $|m = -2\rangle$  states when  $B = 0$  T. This makes  $\Delta m = 0$  transitions (where  $\Delta m$  is the change in  $m$ ) to the  $\psi_1$  state and  $\Delta m = \pm 1$  transitions to the  $\psi_2$  and  $\psi_3$  states strong, whereas transitions to the  $\psi_4$  state are forbidden. At  $B = 7$  T along the N direction (see [Table 1](#)), the situation changes substantially: Because most of the weight in  $\psi_0$  is now in the  $|m = -2\rangle$  state,  $\Delta m = \pm 1$  transitions to the  $\psi_2$  and  $\psi_3$  states remain visible, whereas  $\Delta m = 0$  transitions to the  $\psi_1$  and  $\psi_4$  states are too weak to observe. The  $\Delta m = 0, \pm 1$  requirement implied by Eq. 2 is consistent with previous empirically observed selection rules in STM spin-excitation experiments ([15](#)).

**View this table:**  
[\[in this window\]](#)  
[\[in a new window\]](#)

**Table 1.** Eigenvectors of the spin Hamiltonian for Fe on CuN. A list of eigenvectors, written as a sum of  $|lm\rangle$  states and obtained by diagonalizing Eq. 1 with  $S = 2$ ,  $g = 2.11$ ,  $D = -1.55$  meV, and  $E = 0.31$  meV at  $B = 0$  T and at  $B = 7$  T oriented along the N direction is shown.

The spin-transition matrix element described in Eq. 2 is the same as the matrix element for inelastic neutron scattering in a polycrystalline magnetic system ([31](#)). We suggest that the observed inelastic tunneling arises from similar magnetic interactions between the spin of the tunneling electron and the spin of the magnetic atom—either direct dipolar interactions or through an exchange interaction. The intensity of this inelastic process is remarkably large for a single Fe atom on CuN: At  $B = 0$ , the inelastic conductance (i.e.,

the sum of the IETS steps) is at least as large as the elastic conductance (as measured at  $V = 0$ ). Resonant enhancement of the inelastic tunneling resulting from a coincidence of the relevant orbitals may explain its relative prominence.

We can model the full conductance spectra as the sum of (i) a voltage-independent elastic conductance and (ii) a series of thermally broadened IETS transitions (27) weighted by the transition intensities given in Eq. 2 and by the Boltzmann population of the filled initial and empty final states. A comparison of Fig. 2, B and F, demonstrates the excellent agreement between the measured and calculated spectra. Similar agreement is also seen when  $B$  is oriented in the other directions discussed above [fig. S1C in (28)].

Substantially weaker magnetic anisotropy is observed for Mn atoms on CuN, even though its local chemical environment is very similar to that of Fe. Figure 3A shows IETS spectra obtained for Mn on CuN, with  $B$  oriented out-of-plane; spectra obtained in the two in-plane directions are also shown in fig. S2A (28). Using the spin of a free Mn atom ( $S = \frac{5}{2}$ ) (15), a best fit of the excitation energies from two different Mn atoms on two different CuN islands (Fig. 2B) to Eq. 1 yields  $g = 1.90 \pm 0.01$ ,  $D = -0.039 \pm 0.001$  meV, and  $E = 0.007 \pm 0.001$  meV. As seen in Fig. 3 and fig. S2 (28), agreement between the calculated and observed transition energies and the spectral line shapes is excellent for different Mn atoms in all three orientations of  $B$ . In contrast to the results for Fe, however, these results indicate that the easy axis ( $z$  axis in Eq. 1) for Mn is oriented out-of-plane. A comparison of the DFT calculations of the structures for Fe and Mn on CuN (Figs. 1C and 3C, respectively) shows that they are similar and does not suggest an obvious reason for the change in orientation of the anisotropy axis. The small size of  $D$  is consistent with anisotropy values observed for Mn in molecular magnetic clusters (30).

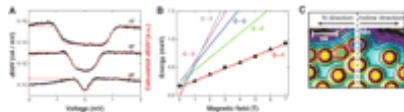


**Fig. 3.** Conductance spectra and structure of Mn atoms on CuN. (A) Spectra (black) taken with the tip positioned above a Mn atom at  $T = 0.5$  K, with the magnetic field oriented out-of-plane. All spectra were acquired at a nominal junction impedance of 10 megohm (10 mV, 1 nA) and are offset by 0.025 nA/mV for clarity. Red lines represent simulated spectra with an effective temperature of 0.7 K. The simulated inelastic spectra are scaled by an overall constant and offset to match the observed spectra. (B) Step energy of two different Mn atoms, indicated by circles and triangles, with  $B$  oriented out-of-plane. Colored lines show the possible transition energies calculated using Eq. 1 with the fit parameters listed in the text for  $B$  along the  $z$  direction. Because the anisotropy parameters are substantially smaller than those for Fe, level

crossings complicate the assignment of the spin excitations at small magnetic fields. (C) Charge density for a Mn atom adsorbed on a CuN surface on Cu(100) calculated by DFT along the N and hollow directions. Solid yellow, green, and blue circles with gray edges label the centers of the Cu, N, and Mn atoms, respectively. The charge-density scale is the same as that shown in [Fig. 1](#). [[View Larger Version of this Image \(17K GIF file\)](#)]

For both Fe and Mn on CuN, we find that the excitation spectrum is well described by a net spin identical to the free-atom spin (i.e.,  $S = 2$  for Fe and  $\frac{5}{2}$  for Mn). For comparison, we performed spin-resolved DFT calculations for these systems and found that most of the net spin is localized on the magnetic atom and the surrounding interstitial region ([25](#)):  $S = 1.73$  for Fe and 2.28 for Mn. However, a substantial amount of spin density extends into the surrounding atoms, as illustrated in [Fig. 4](#) for Fe, where we find that the spin spreading occurs primarily along the N direction in the surface molecular network. By including the spin of all of the atoms, the net spin of the total structure is calculated to be the same as that of the free magnetic atoms:  $S = 2.00$  for Fe and 2.50 for Mn. In comparison, no substantial net spin density is found for bare CuN on Cu(100). This spreading of spin density, here up to 4 Å from the Fe binding site, is similar to that reported in DFT calculations of molecular magnets ([32](#)). Further analysis of the qualitative differences in the spatial distribution of the net spin for the case of Mn and Fe may yield insight into the atomic-scale origins of the differences in their observed anisotropies.

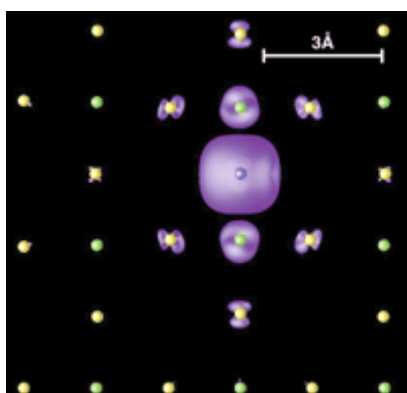


**Fig. 4.** Calculated net-spin-density distribution for Fe on CuN. Contours (purple) of constant net spin density ( $0.01 e/a^3_0$ ), as calculated by DFT for an Fe atom adsorbed on a Cu site on a CuN surface, are shown ([25](#)). Only the Fe atom and the atoms in the CuN surface layer are shown for clarity. Small yellow, green, and blue balls indicate the positions of the Cu, N, and Fe atoms, respectively, in the surface layer. [[View Larger Version of this Image \(34K GIF file\)](#)]

The surface-embedded molecular magnetic structures we have described here are model systems for the study of magnetic anisotropy on surfaces. These structures are similar to molecular magnets because the individual magnetic atoms are incorporated into a

molecular-bonding network. In contrast to molecular magnets, the structures studied here can be constructed, probed, and manipulated atom-by-atom. The results presented here provide a detailed phenomenological picture of the magnetic anisotropy for a single atomic spin in a well-characterized environment. Further theoretical and experimental studies of these systems may allow for the development of a fully microscopic picture of the atomic-scale origins of magnetocrystalline anisotropy. Combining this with the ability to couple atomic spins into extended quantum-spin structures may eventually enable the development of systems in which giant magnetic anisotropy can be completely engineered at the atomic scale.

## References and Notes

- 1. P. Gambardella *et al.*, *Science* **300**, 1130 (2003). [[Abstract/Free Full Text](#)]
- 2. M. Bode, O. Pietzsch, A. Kubetzka, R. Wiesendanger, *Phys. Rev. Lett.* **92**, 067201 (2004). [[CrossRef](#)] [[Medline](#)]
- 3. R. Sessoli, D. Gatteschi, A. Caneschi, M. A. Novak, *Nature* **365**, 141 (1993). [[CrossRef](#)]
- 4. J. R. Long, in *Chemistry of Nanostructured Materials*, P. Yang, Ed. (World Scientific Publishing, Hong Kong, 2003), pp. 241–315.
- 5. D. Gatteschi, R. Sessoli, J. Villain, *Molecular Nanomagnets*, (Oxford Univ. Press, Oxford, 2006).
- 6. R. L. White, *J. Mag. Mag. Mater.* **209**, 1 (2000). [[CrossRef](#)]
- 7. J. R. Friedman, M. P. Sarachik, J. Tejada, R. Ziolo, *Phys. Rev. Lett.* **76**, 3830 (1996). [[CrossRef](#)] [[ISI](#)] [[Medline](#)]
- 8. L. Thomas *et al.*, *Nature* **383**, 145 (1996). [[CrossRef](#)]
- 9. W. Wernsdorfer, R. Sessoli, *Science* **284**, 133 (1999). [[Abstract/Free Full Text](#)]
- 10. M. N. Leuenberger, D. Loss, *Nature* **410**, 789 (2001). [[CrossRef](#)] [[Medline](#)]
- 11. A. Ardavan *et al.*, *Phys. Rev. Lett.* **98**, 057201 (2007). [[CrossRef](#)] [[Medline](#)]
- 12. H. B. Heersche *et al.*, *Phys. Rev. Lett.* **96**, 206801 (2006). [[CrossRef](#)] [[Medline](#)]
- 13. M.-H. Jo *et al.*, *Nano Lett.* **6**, 2014 (2006). [[CrossRef](#)] [[ISI](#)] [[Medline](#)]
- 14. A. J. Heinrich, J. A. Gupta, C. P. Lutz, D. M. Eigler, *Science* **306**, 466 (2004). [[Abstract/Free Full Text](#)]
- 15. C. F. Hirjibehedin, C. P. Lutz, A. J. Heinrich, *Science* **312**, 1021 (2006); published online 29 March 2006 (10.1126/science.1125398). [[Abstract/Free Full Text](#)]
- 16. A. Yamasaki, W. Wulfhekel, R. Hertel, S. Suga, J. Kirschner, *Phys. Rev. Lett.* **91**, 127201 (2003). [[CrossRef](#)] [[Medline](#)]
- 17. H. J. Lee, W. Ho, M. Persson, *Phys. Rev. Lett.* **92**, 186802 (2004). [[CrossRef](#)] [[Medline](#)]
- 18. D. Kitchen, A. Richardella, J.-M. Tang, M. E. Flatté, A. Yazdani, *Nature* **442**, 436 (2006). [[CrossRef](#)] [[Medline](#)]
- 19. In the analysis of the perpendicular orientation, we neglected a  $\sim 7^\circ$  tilt of the sample-surface normal from the magnetic field.

- 20. F. M. Leibsle, S. S. Dhesi, S. D. Barrett, A. W. Robinson, *Surf. Sci.* **317**, 309 (1994). [\[CrossRef\]](#)
- 21. On the CuN surface, Fe and Mn atoms can bind on top of either the Cu atoms or the N atoms. In this work, we considered only the Cu binding site. Atoms were placed away from both defects in and the edges of the CuN islands, where large deviations in magnetic anisotropy may be expected.
- 22. P. Blaha, K. Schwarz, G. Madsen, D. Kvasnicka, J. Luitz, WIEN2k (Technische Univ. Wien, Vienna, 1999).
- 23. J. P. Perdew, K. Burke, M. Ernzerhof, *Phys. Rev. Lett.* **77**, 3865 (1996). [\[CrossRef\]](#) [\[ISI\]](#) [\[Medline\]](#)
- 24. We simulated this surface by a supercell of five-layer slabs (seven layers for bare CuN) separated by eight vacuum layers. Each slab had the CuN monolayers on both sides and three Cu layers in between (five layers of Cu for bare CuN). Fe or Mn atoms were located on top of the CuN surface at  $10.8\text{\AA}$  of lateral separation. The crystal structure was optimized until the forces acting on any atom were below 10 millirydbergs/ $a_0$ , where  $a_0$  is the Bohr radius. For bare CuN, our results are similar to earlier DFT calculations using pseudopotentials (33). To investigate how much strong correlation  $U$  is neglected in GGA, we configured the Fe or Mn atom in the local limit for its 3d electrons. In this limit without hybridization to the other atoms, we calculated the cost in Coulomb energy by moving one electron from the valance to the 3d core (34). We found that  $U = 5$  eV for Mn but was negligible (2 eV) for Fe; therefore, a nonzero  $U$  was used only for Mn.
- 25. From the calculated electronic states of the optimized structure, we obtained the charge on each atom by a Bader analysis (35). We determined the spin by separately calculating the total number of electrons with spin up  $N\uparrow$  and spin down  $N\downarrow$  in a specified volume and then subtracted them to yield  $S = (N\uparrow - N\downarrow)/2$ .
- 26. These excitation energies changed by less than  $\pm 5\%$  for Fe atoms adsorbed on different CuN islands and measured with different tips. This variation may arise from slight changes in the local environment caused by the inherent strain in the CuN islands (36).
- 27. J. Lambe, R. C. Jaklevic, *Phys. Rev.* **165**, 821 (1968). [\[CrossRef\]](#) [\[ISI\]](#)
- 28. Additional results are available on *Science Online*.
- 29. An Fe atom adsorbed on a surface could have  $0 \leq S \leq 5/2$ . However, only  $S = 2$  is consistent with the number of levels required to produce the three observed excitations at  $B = 0$ .
- 30. J. Krzystek, A. Ozarowski, J. Telser, *Coord. Chem. Rev.* **250**, 2308 (2006). [\[CrossRef\]](#)
- 31. R. Caciuffo *et al.*, *Phys. Rev. Lett.* **81**, 4744 (1998). [\[CrossRef\]](#) [\[ISI\]](#)
- 32. A. V. Postnikov, J. Kortus, M. R. Pederson, *Phys. Status Solidi (B)* **243**, 2533 (2006). [\[CrossRef\]](#)
- 33. Y. Yoshimoto, S. Tsuneyuki, *Surf. Sci.* **514**, 200 (2002). [\[CrossRef\]](#)
- 34. G. K. H. Madsen, P. Novák, *Europhys. Lett.* **69**, 777 (2005). [\[CrossRef\]](#) [\[ISI\]](#)
- 35. R. F. W. Bader, *Atoms in Molecules: A Quantum Theory*, (Clarendon, Oxford, 1994).

- 36. S.-Y. Ohno, K. Yagyuu, K. Nakatsuji, F. Komori, *Surf. Sci.* **547**, L871 (2003). [\[CrossRef\]](#)
- 37. I. Horcas *et al.*, *Rev. Sci. Instrum.* **78**, 013705 (2007). [\[CrossRef\]](#) [\[Medline\]](#)
- 38. We thank D. M. Eigler for his mentoring and stimulating discussions; B.J. Melior for his expert technical assistance; and S. Blügel, H. Brune, and R. Sessoli for stimulating discussions. A.F.O. thanks J. M. van Ruitenbeek for his guidance and acknowledges support from the Leiden University Fund; C.-Y.L. is partially funded by NSF grant PHY-0425897; M.T. acknowledges support from the Swiss National Science Foundation; and A.J.H. thanks Office of Naval Research for partial financial support.

---

### Supporting Online Material

[www.sciencemag.org/cgi/content/full/317/5842/1199/DC1](http://www.sciencemag.org/cgi/content/full/317/5842/1199/DC1)

Figs. S1 and S2

---

Received for publication 5 June 2007. Accepted for publication 25 July 2007.

# Large Magnetic Anisotropy of a Single Atomic Spin Embedded in a Surface Molecular Network

Cyrus F. Hirjibehedin,<sup>1</sup> Chiung-Yuan Lin,<sup>1,2</sup> Alexander F. Otte,<sup>1,3</sup> Markus Ternes,<sup>1,4</sup> Christopher P. Lutz,<sup>1</sup> Barbara A. Jones,<sup>1</sup> Andreas J. Heinrich<sup>1</sup>

Magnetic anisotropy allows magnets to maintain their direction of magnetization over time. Using a scanning tunneling microscope to observe spin excitations, we determined the orientation and strength of the anisotropies of individual iron and manganese atoms on a thin layer of copper nitride. The relative intensities of the inelastic tunneling processes are consistent with dipolar interactions, as seen for inelastic neutron scattering. First-principles calculations indicate that the magnetic atoms become incorporated into a polar covalent surface molecular network in the copper nitride. These structures, which provide atom-by-atom accessibility via local probes, have the potential for engineering anisotropies large enough to produce stable magnetization at low temperatures for a single atomic spin.

<sup>1</sup> IBM Research Division, Almaden Research Center, San Jose, CA 95120, USA.

<sup>2</sup> Center for Probing the Nanoscale, Stanford University, Stanford, CA 94309, USA.

<sup>3</sup> Kamerlingh Onnes Laboratorium, Universiteit Leiden, 2300 RA Leiden, Netherlands.

<sup>4</sup> Institut de Physique des Nanostructures, École Polytechnique Fédérale de Lausanne, 1015 Lausanne, Switzerland.

To whom correspondence should be addressed. E-mail: [heinrich@almaden.ibm.com](mailto:heinrich@almaden.ibm.com)

Magnetic structures with only a few atomic spins, such as single atoms and clusters on metal surfaces ([1](#), [2](#)) and molecular magnets ([3–5](#)), can exhibit anisotropies that are large enough to maintain a stable spin orientation at low temperatures. The large anisotropies per each atom in these small clusters are of interest as a possible way to shrink magnetic bits below the size at which domains in current thin-film magnetic materials become unstable at room temperature. The impending approach of this superparamagnetic limit ([6](#)) threatens to halt the decades-long trend toward ever higher storage densities in magnetic memory. Besides this technological relevance, atomic-scale magnetic structures are also of great scientific interest because they exhibit intriguing quantum effects ([7–9](#)) and have the potential to be harnessed for quantum computing ([10](#), [11](#)). Access to individual magnetic nanostructures by electronic transport measurements is possible with the use of electromigration junctions ([12](#), [13](#)) and local probes ([2](#), [14–18](#)). Whereas nanoscale junction devices may be more readily adapted to practical applications, studies using local probes provide an understanding of the nanomagnet's local environment, the crucial determinant of atomic-scale anisotropy.

Here we describe magnetic nanostructures with large magnetic anisotropy that can be individually constructed, studied, and manipulated with atomic-scale precision. Individual Fe or Mn atoms were placed at the desired locations on a CuN surface by manipulation with a scanning tunneling microscope (STM) tip. Our calculations indicate that the Fe and Mn atoms are embedded into a molecular network of polar covalently bonded Cu and

N atoms within the CuN surface. Incorporation into the surface results in substantial charge transfer and distribution of spin polarization away from the magnetic atom and into the molecular network. We found that inelastic excitations of the atomic spin ([14](#), [15](#)) are very prominent in the electron tunneling from an STM tip through the individual magnetic nanostructures. Changes in the spin-excitation energies as a magnetic field was applied along three orthogonal axes directly yielded both the strength and orientation of axial and transverse magnetic anisotropy for a single magnetic atom. The relative intensities of these inelastic excitations are well-described by a spin-transition matrix element that is analogous to that found in inelastic neutron scattering. These nanomagnetic systems combine large magnetic anisotropies with the flexibility that comes from being accessible on a surface by a local probe ([2](#), [14–18](#)) and the potential for control of the magnetic properties previously available only in molecular magnets. This has great promise because, in the absence of transverse anisotropy, the single Fe atom on CuN would have an energy-reversal barrier similar in magnitude to that observed for atomic spins in the most anisotropic configurations in molecular magnets ([4](#)) and on metal surfaces ([1](#)).

Experiments were conducted with an ultra high-vacuum low-temperature STM with a base temperature of 0.5 K. We measured the differential conductance  $dI/dV$  using lock-in detection of the tunnel current  $I$  by adding a 20- to 50- $\mu\text{V}_{\text{rms}}$  modulation at  $\sim 800$  Hz to the sample bias voltage  $V$  [we used the root mean square (rms) amplitude for the modulation voltage]. The STM head was mounted in the cold bore of a split-coil magnet with magnetic fields  $B$  up to 7 T. The orientation of the magnet could be changed so that the magnetic field was applied either perpendicular to or in the plane of the crystal surface ([19](#)).

We used a single atomic layer of CuN ([20](#)) to decouple the spin of the magnetic atoms from the conduction electrons in the underlying Cu(100) surface ([15](#)). A small island of CuN with an adsorbed Fe atom is shown in [Fig. 1A](#). As seen in the cross section, the Fe atom has a large apparent height of 2.6 Å, which indicates that electronic tunneling through the atom is almost three orders of magnitude greater than it is through the bare CuN. The spatial resolution of the STM images, particularly the observation of single rows of missing N atoms such as those shown in [Fig. 1A](#), allowed us to overlay the lattice structure and determine the binding site of the atom and its local environment: In [Fig. 1A](#), the Fe is on top of a Cu atom with two N atoms as its horizontal nearest neighbors ([21](#)).

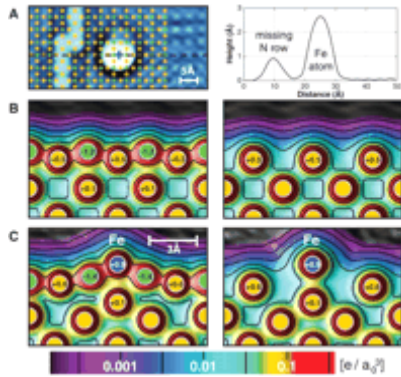


**Fig. 1.** Fe atoms on CuN. (A) (Left) Processed (37) constant-current topograph (10 mV, 0.5 nA) of two adjacent CuN islands with a single adsorbed Fe atom. The topograph is negative-curvature (high-pass) filtered to enhance contrast, with lattice positions of Cu (yellow dots) and N (green dots) atoms overlaid. The light vertical features on the left side of the image are formed by the absence of single rows of N atoms from the CuN surface. The topographic peak of the Fe atom (blue cross) shows its binding site: on top of a Cu site with two N atoms as horizontal neighbors. (Right) Cross section of the unfiltered topograph along the dashed line indicated in the left panel. (B) The charge density for a CuN surface on Cu(100) calculated with the DFT methods described in the text along the N (left) and hollow (right) directions. The scale for the magnitude of the charge density is shown at the bottom in units of  $e/a_0^3$ . Solid yellow and green circles with gray edges label the centers of the Cu and N atoms, respectively. The numbers inside the circles indicate the net charge on selected atoms in units of  $e$  (25). (C) Same as (B) with an Fe atom (blue) adsorbed on the CuN on top of a surface Cu site. [\[View Larger Version of this Image \(96K GIF file\)\]](#)

To understand the structure formed by magnetic atoms on the CuN surface, we calculated the electronic structure using the all-electron full-potential linearized augmented plane wave method of density functional theory (DFT) (22) with the exchange-correlation potential in the generalized gradient approximation (GGA) (23). Figure 1B shows cross sections of the calculated charge density for a single layer of CuN on Cu(100) (24) along two orthogonal directions in-plane: (i) the direction defined by the axis along two nearest-neighbor N atoms (which we refer to below as the N direction) and (ii) the direction along the axis defined by two nearest-neighbor hollow sites (the hollow direction). As seen in the cross sections, the N atoms are slightly above the plane of the surface Cu atoms. In addition, there is a net transfer of charge from the Cu atoms to the N atoms (25). A comparison of the charge densities along the two orientations shows that the CuN has formed a network of polar covalent bonds along the N rows that is distinct from the underlying bulk Cu.

Placing an Fe or Mn atom on top of a Cu atom in the CuN surface causes a substantial rearrangement of the atomic structure. As seen in Fig. 1C for Fe, the Cu atom directly below the magnetic atom has moved toward the bulk and is no longer part of the polar covalent CuN network. The magnetic atom transfers charge to the CuN surface and

creates bonds with its neighboring N atoms; the magnetic atom is thus incorporated into the extended molecular network on the surface. In spite of these extensive structural changes, we can reversibly attach and remove both Fe and Mn atoms from the CuN surface with the STM tip using a previously described technique (15).

The conductance spectra obtained over two different Fe atoms on different CuN islands at various in-plane magnetic fields are shown in Fig. 2, A and B. At  $B = 0$ , three clear steps are seen centered at  $|V_0| \cong 0.2, 3.8,$  and  $5.7$  mV (26). In the framework of inelastic electron tunneling spectroscopy (IETS) (27), these steps in conductance are interpreted as the opening of an inelastic tunneling channel associated with the creation of an excitation at energy  $eV_0$ , where  $e$  is the magnitude of the electron charge and  $V_0$  is the center of the step. Changes in energy and intensity of these excitations as a function of  $B$  allow us to assign them to spin excitations (14, 15). For a single orientation of  $B$ , the atoms were placed at different Cu sites on the surface so that the field was oriented along two different spatial directions: the N direction (for the atom in Fig. 2A) and the hollow direction (Fig. 2B). The existence of zero-field excitations indicates that the different spin orientations (quantum number  $m$ ) are nondegenerate even in the absence of a magnetic field, suggesting the presence of strong magnetic anisotropy in the system even for a single atomic spin on the CuN surface. Surprisingly large magnetic anisotropies have also been observed for isolated metal atoms on bare metal surfaces (1).

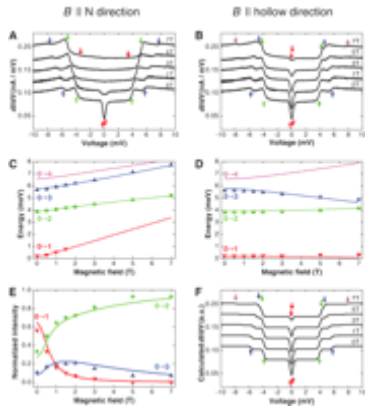


**Fig. 2.** Conductance spectra of Fe atoms on CuN. (A) Spectra taken with the STM tip positioned above an Fe atom at  $T = 0.5$  K and  $B = 0$  to 7 T oriented in the N direction. The spectra were acquired at a nominal junction impedance of 10 megohm (10 mV, 1 nA) and were not sensitive to junction impedance. Successive spectra are vertically offset by 0.023 nA/mV for clarity. Red, green, and blue upward arrows indicate the positions of the first, second, and third excitations, respectively, at  $B = 0$  T as calculated by Eq. 1 with the fit parameters described in the text. Downward arrows show the same excitations at  $B = 7$  T with the magnetic field oriented along the  $z$  axis of Eq. 1. (B) Same as (A) with  $B$  oriented along the hollow direction for the spectra; this direction corresponds to the  $x$  axis of Eq. 1. Also included are magenta downward arrows indicating the calculated position of the fourth transition at  $B = 7$  T. (C) Energies for the first (red triangles), second (green circles), and third (blue triangles) steps observed in the spectra acquired with  $B$  along the N direction, including those shown in (A). Solid lines indicate excitation energies calculated by

Eq. 1 with the magnetic field oriented along the  $z$  axis. **(D)** Step energies for the spectra acquired with  $B$  along the hollow direction, which corresponds to the  $x$  axis of Eq. 1, including those shown in **(B)**. **(E)** Relative step heights for the first (red), second (green), and third (blue) excitations as a function of  $B$  along the N direction. The individual step heights are normalized by the sum of the three step heights at each value of  $B$ . The fourth excitation is not included because its intensities are negligible in this range of  $B$ . Solid lines denote normalized transition intensities calculated using Eq. 2 with the fit parameters discussed in the text. **(F)** Simulated spectra, as described in the text, with  $B$  along the hollow direction and an effective temperature of 0.8 K. Arrows are the same as in **(B)**. These spectra are scaled by an overall constant and offset to match those shown in **(B)**. a.u., arbitrary units. [\[View Larger Version of this Image \(39K GIF file\)\]](#)

In [Fig. 2, C and D](#), the evolution of the energies of the IETS steps seen in [Fig. 2, A and B](#), is shown. The changes in the excitation energies are markedly different when the magnetic field is applied in the two different directions: When  $B$  is along the N direction ([Fig. 2C](#)), all of the step energies increase with  $B$ , whereas the first and third steps decrease in energy when  $B$  is applied along the hollow direction ([Fig. 2D](#)). At a given in-plane magnetic field, it was possible to move an individual Fe atom back and forth between the two distinct binding sites (i.e., sites so that  $B$  was oriented along either the N or hollow direction) and observe that the excitation spectrum switched correspondingly. These differences can be unambiguously observed only because we can probe individual magnetic atoms in a well-characterized environment. A third distinct behavior is seen when the magnetic field is applied in the out-of-plane direction on a different Fe atom, as illustrated in [fig. S1 \(28\)](#); in this case, very little change of the step energies is observed. This strong dependence of the spin excitations on field direction is further evidence of strong magnetic anisotropy for the Fe spin.

To lowest order, spin excitations in an anisotropic environment can be described by the spin Hamiltonian (5)

$$\hat{H} = g\mu_B \vec{B} \cdot \hat{S} + DS_z^2 + E(S_x^2 - S_y^2) \quad (1)$$

Here the first term is the Zeeman splitting of the states in the presence of a magnetic field, where  $g$  is the  $g$ -factor,  $\mu_B$  is the Bohr magneton, and  $\hat{S} = (\hat{S}_x, \hat{S}_y, \hat{S}_z)$  is the spin operator.

The second and third terms are phenomenological representations of the axial and transverse magnetic anisotropies, characterized by strengths  $D$  and  $E$ , respectively. The axial term splits the degeneracy of the spin-states on the basis of the magnitude of the spin's  $z$  projection  $m$ , whereas the transverse term mixes states of different  $m$ . By convention, the axes are assigned in Eq. 1 to maximize  $|D|$  and have  $E > 0$ .

Diagonalization of Eq. 1 allows us to calculate the excitation spectrum for the spin system. Using the spin of a free Fe atom ( $S = 2$ ) (29), a best fit of all of the excitations shown in Fig. 2, C and D, and fig. S1B (28) yields  $g = 2.11 \pm 0.05$ ,  $D = -1.55 \pm 0.01$  meV, and  $E = 0.31 \pm 0.01$  meV; here the uncertainties are the standard errors produced by the best fit.  $D < 0$  favors high  $|m|$  states, which are desirable for achieving magnetic bistability with a long lifetime (4). However, the relatively large transverse  $E$  term mixes the different spins states, making these structures unsuitable for use as bistable spin systems. It may be possible to remove such mixing by engineering the local environment of the atomic spin, for example, by positioning the magnetic atom on a surface site with higher symmetry. Similar magnetic-anisotropy values, although usually with positive  $D$  (corresponding to planar or hard-axis anisotropy), have been observed in studies of crystals formed from molecular magnet structures with single Fe atoms (30).

Figure 2, C and D, and fig. S1B (28) show the agreement between the observed IETS step energies and the excitation energies calculated from Eq. 1 as a function of  $B$ . In these calculations, the direction of  $B$  along the N, hollow, and out-of-plane directions is associated with the  $z$ ,  $x$ , and  $y$  axes in Eq. 1, respectively. A fourth excitation at a higher energy is also predicted to occur. Although no indication of this excitation is observed for  $B$  along the N and out-of-plane directions, a weak conductance step at the predicted energies is observed at larger magnetic fields applied along the hollow direction, as seen in Fig. 2B. Unexpectedly, the primary anisotropy axis (corresponding to the  $z$  axis in Eq. 1) is not directed out-of-plane but rather along the inplane N direction (i.e., along the direction of the CuN molecular network). This result indicates the importance of the local molecular-bonding environment in determining the magnetocrystalline anisotropy.

To better understand the inelastic tunneling process that governs the spin excitations observed with IETS, we also analyzed the intensity of the transitions as a function of magnetic-field strength and orientation. In Fig. 2E, the relative intensities of the three strong IETS steps as a function of  $B$  along the N direction are shown. We found that the relative IETS step heights for transitions between an initial spin eigenstate  $\psi_i$  and a final spin eigenstate  $\psi_f$  are well-described by

$$I_{i \rightarrow f} = \left| \langle \Psi_f | \hat{S}_x | \Psi_i \rangle \right|^2 + \left| \langle \Psi_f | \hat{S}_y | \Psi_i \rangle \right|^2 + \quad (2)$$

$$\begin{aligned}
& \left| \langle \Psi_f | \hat{S}_z | \Psi_i \rangle \right|^2 \\
&= \frac{1}{2} \left[ \left| \langle \Psi_f | \hat{S}_+ | \Psi_i \rangle \right|^2 + \left| \langle \Psi_f | \hat{S}_- | \Psi_i \rangle \right|^2 + \right. \\
& \quad \left. 2 \left| \langle \Psi_f | \hat{S}_z | \Psi_i \rangle \right|^2 \right]
\end{aligned}$$

where  $\hat{S}_\pm = \hat{S}_x \pm i \hat{S}_y$  (here,  $i = \sqrt{-1}$ ) and  $\psi_i$  and  $\psi_f$  are obtained directly from the diagonalization of Eq. 1. As shown in [Table 1](#),  $\psi_0$  has most of its weight in the  $|m = +2\rangle$  and  $| -2\rangle$  states when  $B = 0$  T. This makes  $\Delta m = 0$  transitions (where  $\Delta m$  is the change in  $m$ ) to the  $\psi_1$  state and  $\Delta m = \pm 1$  transitions to the  $\psi_2$  and  $\psi_3$  states strong, whereas transitions to the  $\psi_4$  state are forbidden. At  $B = 7$  T along the N direction (see [Table 1](#)), the situation changes substantially: Because most of the weight in  $\psi_0$  is now in the  $| -2\rangle$  state,  $\Delta m = \pm 1$  transitions to the  $\psi_2$  and  $\psi_3$  states remain visible, whereas  $\Delta m = 0$  transitions to the  $\psi_1$  and  $\psi_4$  states are too weak to observe. The  $\Delta m = 0, \pm 1$  requirement implied by Eq. 2 is consistent with previous empirically observed selection rules in STM spin-excitation experiments ([15](#)).

**View this table:**  
[\[in this window\]](#)  
[\[in a new window\]](#)

**Table 1.** Eigenvectors of the spin Hamiltonian for Fe on CuN. A list of eigenvectors, written as a sum of  $|lm\rangle$  states and obtained by diagonalizing Eq. 1 with  $S = 2$ ,  $g = 2.11$ ,  $D = -1.55$  meV, and  $E = 0.31$  meV at  $B = 0$  T and at  $B = 7$  T oriented along the N direction is shown.

The spin-transition matrix element described in Eq. 2 is the same as the matrix element for inelastic neutron scattering in a polycrystalline magnetic system ([31](#)). We suggest that the observed inelastic tunneling arises from similar magnetic interactions between the spin of the tunneling electron and the spin of the magnetic atom—either direct dipolar interactions or through an exchange interaction. The intensity of this inelastic process is remarkably large for a single Fe atom on CuN: At  $B = 0$ , the inelastic conductance (i.e.,

the sum of the IETS steps) is at least as large as the elastic conductance (as measured at  $V = 0$ ). Resonant enhancement of the inelastic tunneling resulting from a coincidence of the relevant orbitals may explain its relative prominence.

We can model the full conductance spectra as the sum of (i) a voltage-independent elastic conductance and (ii) a series of thermally broadened IETS transitions (27) weighted by the transition intensities given in Eq. 2 and by the Boltzmann population of the filled initial and empty final states. A comparison of Fig. 2, B and F, demonstrates the excellent agreement between the measured and calculated spectra. Similar agreement is also seen when  $B$  is oriented in the other directions discussed above [fig. S1C in (28)].

Substantially weaker magnetic anisotropy is observed for Mn atoms on CuN, even though its local chemical environment is very similar to that of Fe. Figure 3A shows IETS spectra obtained for Mn on CuN, with  $B$  oriented out-of-plane; spectra obtained in the two in-plane directions are also shown in fig. S2A (28). Using the spin of a free Mn atom ( $S = \frac{5}{2}$ ) (15), a best fit of the excitation energies from two different Mn atoms on two different CuN islands (Fig. 2B) to Eq. 1 yields  $g = 1.90 \pm 0.01$ ,  $D = -0.039 \pm 0.001$  meV, and  $E = 0.007 \pm 0.001$  meV. As seen in Fig. 3 and fig. S2 (28), agreement between the calculated and observed transition energies and the spectral line shapes is excellent for different Mn atoms in all three orientations of  $B$ . In contrast to the results for Fe, however, these results indicate that the easy axis ( $z$  axis in Eq. 1) for Mn is oriented out-of-plane. A comparison of the DFT calculations of the structures for Fe and Mn on CuN (Figs. 1C and 3C, respectively) shows that they are similar and does not suggest an obvious reason for the change in orientation of the anisotropy axis. The small size of  $D$  is consistent with anisotropy values observed for Mn in molecular magnetic clusters (30).

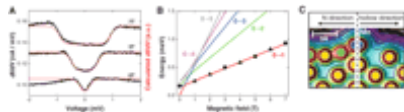


**Fig. 3.** Conductance spectra and structure of Mn atoms on CuN. (A) Spectra (black) taken with the tip positioned above a Mn atom at  $T = 0.5$  K, with the magnetic field oriented out-of-plane. All spectra were acquired at a nominal junction impedance of 10 megohm (10 mV, 1 nA) and are offset by 0.025 nA/mV for clarity. Red lines represent simulated spectra with an effective temperature of 0.7 K. The simulated inelastic spectra are scaled by an overall constant and offset to match the observed spectra. (B) Step energy of two different Mn atoms, indicated by circles and triangles, with  $B$  oriented out-of-plane. Colored lines show the possible transition energies calculated using Eq. 1 with the fit parameters listed in the text for  $B$  along the  $z$  direction. Because the anisotropy parameters are substantially smaller than those for Fe, level

crossings complicate the assignment of the spin excitations at small magnetic fields. (C) Charge density for a Mn atom adsorbed on a CuN surface on Cu(100) calculated by DFT along the N and hollow directions. Solid yellow, green, and blue circles with gray edges label the centers of the Cu, N, and Mn atoms, respectively. The charge-density scale is the same as that shown in [Fig. 1](#). [[View Larger Version of this Image \(17K GIF file\)](#)]

For both Fe and Mn on CuN, we find that the excitation spectrum is well described by a net spin identical to the free-atom spin (i.e.,  $S = 2$  for Fe and  $\frac{5}{2}$  for Mn). For comparison, we performed spin-resolved DFT calculations for these systems and found that most of the net spin is localized on the magnetic atom and the surrounding interstitial region ([25](#)):  $S = 1.73$  for Fe and 2.28 for Mn. However, a substantial amount of spin density extends into the surrounding atoms, as illustrated in [Fig. 4](#) for Fe, where we find that the spin spreading occurs primarily along the N direction in the surface molecular network. By including the spin of all of the atoms, the net spin of the total structure is calculated to be the same as that of the free magnetic atoms:  $S = 2.00$  for Fe and 2.50 for Mn. In comparison, no substantial net spin density is found for bare CuN on Cu(100). This spreading of spin density, here up to 4 Å from the Fe binding site, is similar to that reported in DFT calculations of molecular magnets ([32](#)). Further analysis of the qualitative differences in the spatial distribution of the net spin for the case of Mn and Fe may yield insight into the atomic-scale origins of the differences in their observed anisotropies.

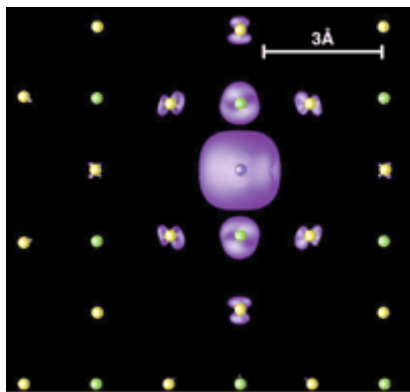


**Fig. 4.** Calculated net-spin-density distribution for Fe on CuN. Contours (purple) of constant net spin density ( $0.01 e/a^3_0$ ), as calculated by DFT for an Fe atom adsorbed on a Cu site on a CuN surface, are shown ([25](#)). Only the Fe atom and the atoms in the CuN surface layer are shown for clarity. Small yellow, green, and blue balls indicate the positions of the Cu, N, and Fe atoms, respectively, in the surface layer. [[View Larger Version of this Image \(34K GIF file\)](#)]

The surface-embedded molecular magnetic structures we have described here are model systems for the study of magnetic anisotropy on surfaces. These structures are similar to molecular magnets because the individual magnetic atoms are incorporated into a

molecular-bonding network. In contrast to molecular magnets, the structures studied here can be constructed, probed, and manipulated atom-by-atom. The results presented here provide a detailed phenomenological picture of the magnetic anisotropy for a single atomic spin in a well-characterized environment. Further theoretical and experimental studies of these systems may allow for the development of a fully microscopic picture of the atomic-scale origins of magnetocrystalline anisotropy. Combining this with the ability to couple atomic spins into extended quantum-spin structures may eventually enable the development of systems in which giant magnetic anisotropy can be completely engineered at the atomic scale.

## References and Notes

- 1. P. Gambardella *et al.*, *Science* **300**, 1130 (2003). [[Abstract/Free Full Text](#)]
- 2. M. Bode, O. Pietzsch, A. Kubetzka, R. Wiesendanger, *Phys. Rev. Lett.* **92**, 067201 (2004). [[CrossRef](#)] [[Medline](#)]
- 3. R. Sessoli, D. Gatteschi, A. Caneschi, M. A. Novak, *Nature* **365**, 141 (1993). [[CrossRef](#)]
- 4. J. R. Long, in *Chemistry of Nanostructured Materials*, P. Yang, Ed. (World Scientific Publishing, Hong Kong, 2003), pp. 241–315.
- 5. D. Gatteschi, R. Sessoli, J. Villain, *Molecular Nanomagnets*, (Oxford Univ. Press, Oxford, 2006).
- 6. R. L. White, *J. Mag. Mag. Mater.* **209**, 1 (2000). [[CrossRef](#)]
- 7. J. R. Friedman, M. P. Sarachik, J. Tejada, R. Ziolo, *Phys. Rev. Lett.* **76**, 3830 (1996). [[CrossRef](#)] [[ISI](#)] [[Medline](#)]
- 8. L. Thomas *et al.*, *Nature* **383**, 145 (1996). [[CrossRef](#)]
- 9. W. Wernsdorfer, R. Sessoli, *Science* **284**, 133 (1999). [[Abstract/Free Full Text](#)]
- 10. M. N. Leuenberger, D. Loss, *Nature* **410**, 789 (2001). [[CrossRef](#)] [[Medline](#)]
- 11. A. Ardavan *et al.*, *Phys. Rev. Lett.* **98**, 057201 (2007). [[CrossRef](#)] [[Medline](#)]
- 12. H. B. Heersche *et al.*, *Phys. Rev. Lett.* **96**, 206801 (2006). [[CrossRef](#)] [[Medline](#)]
- 13. M.-H. Jo *et al.*, *Nano Lett.* **6**, 2014 (2006). [[CrossRef](#)] [[ISI](#)] [[Medline](#)]
- 14. A. J. Heinrich, J. A. Gupta, C. P. Lutz, D. M. Eigler, *Science* **306**, 466 (2004). [[Abstract/Free Full Text](#)]
- 15. C. F. Hirjibehedin, C. P. Lutz, A. J. Heinrich, *Science* **312**, 1021 (2006); published online 29 March 2006 (10.1126/science.1125398). [[Abstract/Free Full Text](#)]
- 16. A. Yamasaki, W. Wulfhekel, R. Hertel, S. Suga, J. Kirschner, *Phys. Rev. Lett.* **91**, 127201 (2003). [[CrossRef](#)] [[Medline](#)]
- 17. H. J. Lee, W. Ho, M. Persson, *Phys. Rev. Lett.* **92**, 186802 (2004). [[CrossRef](#)] [[Medline](#)]
- 18. D. Kitchen, A. Richardella, J.-M. Tang, M. E. Flatté, A. Yazdani, *Nature* **442**, 436 (2006). [[CrossRef](#)] [[Medline](#)]
- 19. In the analysis of the perpendicular orientation, we neglected a  $\sim 7^\circ$  tilt of the sample-surface normal from the magnetic field.

- 20. F. M. Leibsle, S. S. Dhesi, S. D. Barrett, A. W. Robinson, *Surf. Sci.* **317**, 309 (1994). [\[CrossRef\]](#)
- 21. On the CuN surface, Fe and Mn atoms can bind on top of either the Cu atoms or the N atoms. In this work, we considered only the Cu binding site. Atoms were placed away from both defects in and the edges of the CuN islands, where large deviations in magnetic anisotropy may be expected.
- 22. P. Blaha, K. Schwarz, G. Madsen, D. Kvasnicka, J. Luitz, WIEN2k (Technische Univ. Wien, Vienna, 1999).
- 23. J. P. Perdew, K. Burke, M. Ernzerhof, *Phys. Rev. Lett.* **77**, 3865 (1996). [\[CrossRef\]](#) [\[ISI\]](#) [\[Medline\]](#)
- 24. We simulated this surface by a supercell of five-layer slabs (seven layers for bare CuN) separated by eight vacuum layers. Each slab had the CuN monolayers on both sides and three Cu layers in between (five layers of Cu for bare CuN). Fe or Mn atoms were located on top of the CuN surface at  $10.8\text{\AA}$  of lateral separation. The crystal structure was optimized until the forces acting on any atom were below 10 millirydbergs/ $a_0$ , where  $a_0$  is the Bohr radius. For bare CuN, our results are similar to earlier DFT calculations using pseudopotentials (33). To investigate how much strong correlation  $U$  is neglected in GGA, we configured the Fe or Mn atom in the local limit for its 3d electrons. In this limit without hybridization to the other atoms, we calculated the cost in Coulomb energy by moving one electron from the valance to the 3d core (34). We found that  $U = 5$  eV for Mn but was negligible (2 eV) for Fe; therefore, a nonzero  $U$  was used only for Mn.
- 25. From the calculated electronic states of the optimized structure, we obtained the charge on each atom by a Bader analysis (35). We determined the spin by separately calculating the total number of electrons with spin up  $N\uparrow$  and spin down  $N\downarrow$  in a specified volume and then subtracted them to yield  $S = (N\uparrow - N\downarrow)/2$ .
- 26. These excitation energies changed by less than  $\pm 5\%$  for Fe atoms adsorbed on different CuN islands and measured with different tips. This variation may arise from slight changes in the local environment caused by the inherent strain in the CuN islands (36).
- 27. J. Lambe, R. C. Jaklevic, *Phys. Rev.* **165**, 821 (1968). [\[CrossRef\]](#) [\[ISI\]](#)
- 28. Additional results are available on *Science Online*.
- 29. An Fe atom adsorbed on a surface could have  $0 \leq S \leq 5/2$ . However, only  $S = 2$  is consistent with the number of levels required to produce the three observed excitations at  $B = 0$ .
- 30. J. Krzystek, A. Ozarowski, J. Telser, *Coord. Chem. Rev.* **250**, 2308 (2006). [\[CrossRef\]](#)
- 31. R. Caciuffo *et al.*, *Phys. Rev. Lett.* **81**, 4744 (1998). [\[CrossRef\]](#) [\[ISI\]](#)
- 32. A. V. Postnikov, J. Kortus, M. R. Pederson, *Phys. Status Solidi (B)* **243**, 2533 (2006). [\[CrossRef\]](#)
- 33. Y. Yoshimoto, S. Tsuneyuki, *Surf. Sci.* **514**, 200 (2002). [\[CrossRef\]](#)
- 34. G. K. H. Madsen, P. Novák, *Europhys. Lett.* **69**, 777 (2005). [\[CrossRef\]](#) [\[ISI\]](#)
- 35. R. F. W. Bader, *Atoms in Molecules: A Quantum Theory*, (Clarendon, Oxford, 1994).

- 36. S.-Y. Ohno, K. Yagyuu, K. Nakatsuji, F. Komori, *Surf. Sci.* **547**, L871 (2003). [\[CrossRef\]](#)
- 37. I. Horcas *et al.*, *Rev. Sci. Instrum.* **78**, 013705 (2007). [\[CrossRef\]](#) [\[Medline\]](#)
- 38. We thank D. M. Eigler for his mentoring and stimulating discussions; B.J. Melior for his expert technical assistance; and S. Blügel, H. Brune, and R. Sessoli for stimulating discussions. A.F.O. thanks J. M. van Ruitenbeek for his guidance and acknowledges support from the Leiden University Fund; C.-Y.L. is partially funded by NSF grant PHY-0425897; M.T. acknowledges support from the Swiss National Science Foundation; and A.J.H. thanks Office of Naval Research for partial financial support.

---

### Supporting Online Material

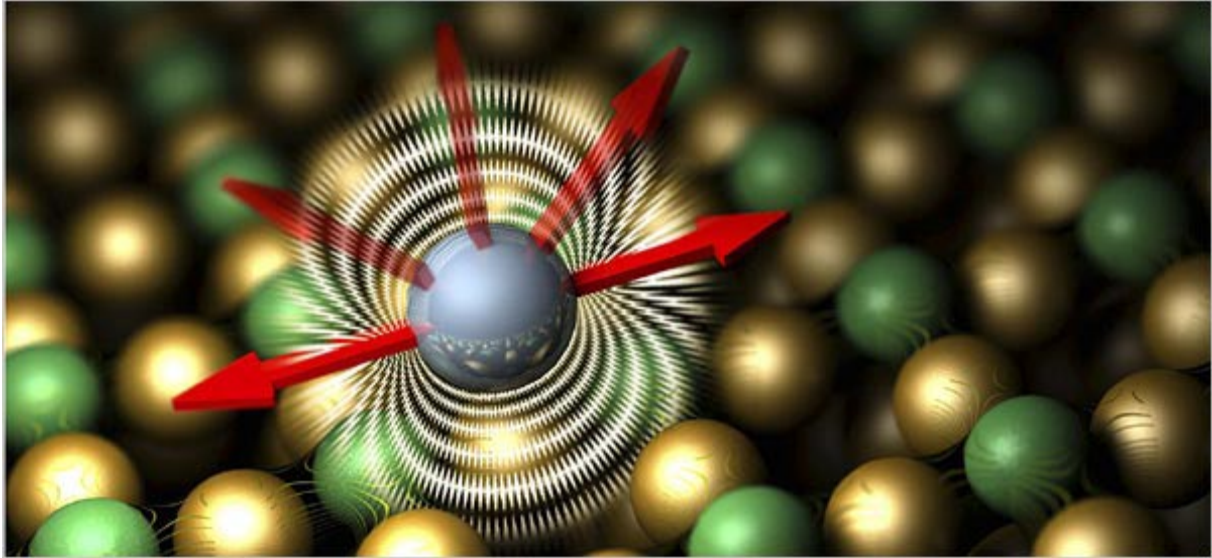
[www.sciencemag.org/cgi/content/full/317/5842/1199/DC1](http://www.sciencemag.org/cgi/content/full/317/5842/1199/DC1)

Figs. S1 and S2

---

Received for publication 5 June 2007. Accepted for publication 25 July 2007.

## I.B.M. Researchers Advancing Computer Processing Ability



I.B.M.

An illustration of I.B.M.'s technique for storing data on a single atom. An iron atom on a copper surface could store a single bit of binary data, with "0" or "1" indicated by the orientation of the atom's magnetic field.

By [JOHN MARKOFF](#)

Published: August 31, 2007

SAN FRANCISCO, Aug. 30 — Researchers at [I.B.M.](#) laboratories say they have made progress toward storing information and computing at the level of individual atoms.

The scientists documented their work in two papers appearing on Friday in the journal *Science*. Both papers are focused on new understanding of the behavior of magnetism at the tiny scale of nanotechnology, where scientists hope to develop electronics made from components that are far smaller than today's transistors and wires.

[In one paper](#) the researchers describe a technique for reading and writing digital ones and zeroes onto a handful of atoms, or even individual atoms. [The second paper](#) describes the ability to use a single molecule as a switch, replicating the behavior of today's transistors.

The papers are the latest indication that computing technology is beginning to emerge that could replace today's microelectronics materials in the next decade.

R. Stanley Williams, a [Hewlett-Packard](#) physicist, said this week that his group had begun manufacturing prototypes of a silicon chip that combines both conventional microelectronics and molecular scale components. Their first hybrid device is a circuit called a field programmable gate array, or F.P.G.A., using molecular-scale components

as the configuration circuitry, an approach that will save tremendous space in the chip design.

A team of I.B.M. researchers at the company's Almaden Research Center in San Jose, Calif., were able to use a scanning tunneling microscope to observe the magnetic orientation of iron and manganese atoms at low temperatures. Controlling magnetic direction is a crucial technique that is used in reading and writing digital information on magnetic storage disks like standard hard drives.

In addition to the potential storage applications, the researchers noted that atomic-scale magnetic structures are also of scientific interest because they may be harnessed for quantum computing, a technology that would be far faster than current computers for some specialized uses.

A second group of I.B.M. scientists in Zurich were able to place two hydrogen atoms in an ultrathin insulating film and switch them back and forth between two states, creating the equivalent of the ones and zeroes used in standard chips. They were also able to use the same switching process to inject an electric charge into one molecule and link the effect to a neighboring molecule. That suggests it might be possible to extend the effect into a fabric of trillions of atom-size switches in the future.

The laboratory advances are far from being ready to commercialize, but they provide hope for the electronics industry, which has grown steadily because of the continuous shrinking in size and falling cost of components for more than four decades.